RESEARCH ON THE TRANSONIC AEROFOIL SECTIONS AT THE NATIONAL AEROSPACE LABORATORY, JAPAN

Takashi Shigemi
Chief, the Second Aerodynamics Division
National Aerospace Laboratory
Tokyo, Japan

Abstract

A brief review is made of the recent studies on transonic aerofoil sections performed in NAL, Japan.

It was found that we can obtain exact solutions for the flow past various aerofoil sections if we only superpose additional functions to the well-established hodograph solution for the lifting circular cylinder. Various sections have been computed until now; some of them were tested in 2m. transonic wind tunnel and results showed a good agreement with the theory.

An additional remark is given on empirical procedures developed in parallel with the above theory, which furnish us with a quick access to the aerofoil design problem.

1. Introduction

The study on the transonic aerofoil problem started in NAL in 1966 around, when we were informed of the concept of 'peaky' aerofoil sections originated by Pearcey[1]. This problem seemed so attractive to us that we started various experimental trials in order at least to understand and realize this new concept. As this concept implied a shock-free (isentropic) flow around an aerofoil, we thought that a theoretical approach would be feasible as well. Hence re-examined were the classical theories including exact theories of Lighthill[2,3,4] and Cherry[5] as well as other approximate theories.

In 1967, we were favoured with a copy of Nieuwland's paper[6] from which we learned that Lighthill's theory had actually been applied by him to the theoretical design of transonic aerofoil sections. Later information revealed that a series of symmetrical 'quasi-elliptical' sections had been already computed by Boerstoel[7] and published in a form of catalogue. As we thought that NLR's work was almost complete and that we could not add anything of importance, we gave up our effort to investigate symmetrical (non-lifting) sections. As to the lifting aerofoils, however, Nieuwland had shown only his procedure of theoretical computation at that time[8], and we had a feeling that his theory involved too much complication. Hence we decided first to concentrate in building up a theory for a lifting aerofoil based on a different standpoint, aiming at a mathematically rigorous theory all the same.

In 1970, we completed the theory together with the computer program for the calculation of aerofoil sections; most of them were worked out by Takanashi[9]. The outline of this theory will be described in Section 2, and the results of wind-tunnel tests of the aerofoil sections obtained by this method will be described in Section 3.

At the time we started the above investigation, we anticipated that it would take naturally a long time to accomplish it. Hence we considered an alternative approach in parallel. This was an empirical process using well-established techniques in the low-speed aerofoil theory, the Prandtl-Glauert rule, and sometimes an empirical relationship between subcritical and transonic characteristics of an aerofoil. A short comment on this empirical method will be given in Section 4.

2. Theoretical Work Based upon Hodograph Method

2.1 The Concept of the Hodograph Method

In the present paper, the author does not intend to enter the mathematical detail, but a short introductory comment on the classical hodograph method must be necessary.

The hodograph equation for the stream function Ψ of the two-dimentional potential flow of a compressible fluid, on the assumption of isentropic gas law, can be written as:

$$\tau(1-\tau)\frac{\partial^2\psi}{\partial\tau^2} + \left(1+\frac{2-\gamma}{\gamma-1}\tau\right)\frac{\partial\psi}{\partial\tau} + \frac{1}{4\tau}\left(1-\frac{\gamma+1}{\gamma-1}\tau\right)\frac{\partial^2\psi}{\partial\theta^2} = 0 \quad , \tag{1}$$

where

$$\tau = \left(\frac{q}{q_{max}}\right)^2 = \frac{1}{1+\frac{2}{\gamma-1}\frac{1}{M^2}} \quad ,$$

q and θ are the magnitude and inclination (to the axis of reference) of the local velocity of the flow; q_{max} is the limit speed; M is the local Mach number; and γ is the ratio of the specific-heats.

We want to construct the flow field by superposition of the following Chaplygin's solution for Eq.1:

$$\psi_\nu(\tau)\, e^{\pm i\nu\theta} \tag{2}$$

where

$$\psi_\nu(\tau) = \tau^{\nu/2}\, F(a_\nu, b_\nu;\ \nu+1;\ \tau) \tag{3}$$

$$a_\nu + b_\nu = \nu - \frac{1}{\gamma-1} \quad , \quad a_\nu b_\nu = \frac{-\nu(\nu+1)}{2(\gamma-1)} \quad . \tag{4}$$

In these expressions, F is a hypergeometric function that is regular at the point $\tau=0$; and ν denotes an arbitrary complex number, negative integers $-2, -3, -4, \cdots$ being excluded.

Now, let us assume that the complex velocity potential w of an incompressible flow past an obstacle can be expressed in terms of the complex velocity $\zeta = qe^{-i\theta}$ by the integral*

$$w(\zeta) = \frac{1}{2\pi i}\int_{-i\infty}^{i\infty} G(\nu)(-\zeta)^{\nu} d\nu \ , \qquad (5)$$

where $G(\nu)$ is a meromorphic function of the complex variable ν, and may be determined from $w(\zeta)$ in a closed form by use of Mellin-transform theorems[8]. The compressible-flow solution corresponding to the above incompressible counterpart is then given, in the form of the stream function Ψ, as:

$$\Psi = \mathrm{Im.}[W],$$

$$W = \frac{1}{2\pi i}\int_{-i\infty}^{i\infty} G(\nu)\, f_{\nu}(\tau_1)\psi_{\nu}(\tau)(-1)^{\nu} e^{-i\nu\theta} d\nu \ . \qquad (6)$$

In this expression, τ_1 is the value of τ corresponding to the speed at infinity in the physical plane, which is assumed to be subsonic and taken as unity for convenience' sake, i.e. $\tau_1 = (1/q_{max})^2$; on the other hand, $f_{\nu}(\tau_1)$ is the so-called compressibility factor satisfying following conditions[2]:
(i) $f_{\nu}(\tau_1)$ is a meromorphic function of ν, having at most simple poles with real residues on the real axis exclusive of 0, -1, -2, -3, ...
(ii) $f_{\nu}(\tau_1) \sim \tau_1^{-\nu/2}$, as $\tau_1 \to 0$.
(iii) There exists a function $A(\tau_1)$ such that $f_{\nu}(\tau_1) \sim A(\tau_1)e^{-\nu s_1}$ as $\nu \to \infty$, where

$$s_1 = s(\tau_1),$$

$$s(\tau) = -\sqrt{\frac{\gamma+1}{\gamma-1}}\tanh^{-1}\sqrt{\frac{\gamma-1}{\gamma+1}} + \frac{1}{2}\log(2\gamma-2)$$

$$+\sqrt{\frac{\gamma+1}{\gamma-1}}\tanh^{-1}\sqrt{\frac{\gamma-1-(\gamma+1)\tau}{(\gamma+1)(1-\tau)}} - \tanh^{-1}\sqrt{\frac{\gamma-1-(\gamma+1)\tau}{(\gamma-1)(1-\tau)}}$$

$$\sim \frac{1}{2}\log\tau \quad (\tau \to 0). \qquad (7)$$

Condition (ii) ensures that the compressible-flow function (6) tends to the original incompressible-flow function (5) as the uniform-flow Mach number approaches zero, since $f_{\nu}(\tau_1)\psi_{\nu}(\tau) \sim \tau_1^{-\nu/2}\tau^{\nu/2} = q^{\nu}$ as $q_{max} \to \infty$. Meanwhile, condition (iii) ensures that the integrand in Eq. 6 behaves, in the subsonic region, like that in Eq. 5 in the limit $\nu \to \infty$; and, in particular, the behaviour of the former near $\tau = \tau_1$ is identical to that of the latter near $q = 1$, since $\psi_{\nu}(\tau)$ is asymptotically equal to $V(\tau)e^{\nu s}$ as $\nu \to \infty$ for a subsonic speed $\tau < (\gamma-1)/(\gamma+1)$. ($V(\tau)$ is also a function of τ.)

The Chaplygin function $\psi_{\nu}(\tau)$ is also a meromorphic function of ν, which has only simple poles at $\nu = -2, -3, -4, \ldots$; hence the integral in Eq. 6 can be evaluated by the residue theorem yielding series expansions which are valid in different regions of convergence in the hodograph plane. The series expansion also provides the means of extension of the solution to the supersonic region.

2.2 The Generating Function

As we have seen in Section 2.1, the compressible-flow function (6) can be constructed from the incompressible-flow function if the latter may be expressed in either a series form or an integral form (5). This approach has been taken by many investigators, starting from incompressible flows past simple-shaped obstacles such as circular[2,3,4,5] and elliptic[6,8] cylinders, including non-lifting and lifting cases (see CASE I~IV, Table 1).

As we are starting from an incompressible flow in this approach, we can get at least some notion of the final shape of the obstacle even though it suffers a considerable change in the course of incompressible-to-compressible transformation; and above all, we can have a precise knowledge of the singularities of the flow that must be preserved through the transformation to the compressible flow. The hodograph plane of the flow past an obstacle is in most typical cases composed of two sheets of the Riemann surface. If it concerns a flow past a non-lifting body, the essential singularity in question is of the type:

$$w \sim (1-\zeta)^{-1/2} \qquad (8)$$

located at the point $\zeta = 1$ which corresponds to $z = \infty$ in the physical plane. It represents a branch point there, and also a dipole covering an angular range of 4π (spreading over two sheets of Riemann surface). If the flow involves circulation Γ, on the other hand, the branch point is located at another point $\zeta = \zeta_2$, say, which corresponds to a finite point in the physical (z-) plane; while to the point $z = \infty$ corresponds the point $\zeta = 1$ on only one sheet (tentatively named as the 'upper sheet') of the Riemann surface, and there the complex velocity-potential w has a singularity of dipole and vortex which is expressed as:

$$w \sim -\frac{i\Gamma}{2\pi}\left\{\frac{1}{1-\zeta} + \log(1-\zeta)\right\} . \qquad (9)$$

Note that the flow is regular at the point $\zeta = 1$ on the other sheet(the 'lower sheet').

Such are the only singularities (except the complementary singurarities at $\zeta = \infty$) which appear in the hodograph plane when one deals with the flow past a circular cylinder; if one treats more complicated flow, however, other singularities would naturally appear. In the case of an elliptic cylinder, for instance, there comes at $\zeta = 1/\varepsilon$ (ε denotes the eccentricity of the ellipse) an additional singularity which is similar to the one at $\zeta = 1$; for the lifting case, still another singularity (a branch point) appears at $\zeta = \zeta_2'$, say, which is similar to that at $\zeta = \zeta_2$. Due to these additional singularities the formulation of the solution for an elliptic cylinder is much more complicated. We owe Nieuwland for his laborious works[6,8] on the solution for an elliptic cylinder.

Now, neither the elliptic nor the circular cylinder is a shape of particular interest to the practical aerofoil design. Working with an elliptic cylinder, however, one can get possession of a new arbitrary parameter ε which is useful in varying the thickness-ratio of the resulting profile. In addition to that, Nieuwland[6] used a certain series solution of the fundamental equation (1), which was superposed to the original solution for an elliptic cylinder in order to 'unbalance' the flow conditions at the front and rear parts of the aerofoil, hence adjusting the leading-edge radius and also eliminating the formation of a cusped

* The development of the theory is also possible if $w(\zeta)$ is expressed in a series form. In this paper, however, the integral form (5) is preferred for the sake of consistency.

Table 1. SCHEME OF INCOMPRESSIBLE-TO-COMPRESSIBLE TRANSFORMATION IN THE HODOGRAPH METHOD
(With particular use of compressibility factor $f_\nu(\tau_1) = e^{-\nu s_1}$ or $\{\psi_{-\nu}(\tau_1)+2\tau_1\psi'_{-\nu}(\tau_1)\}/(1-\nu)$.)

CASE	Classification of the Generating Flow	INCOMPRESSIBLE FLOW FUNCTION (w)			COMPRESSIBLE FLOW FUNCTION (W)
		In Physical Plane (z-pl)	In Hodograph Plane (ζ-plane)		In Hodograph Plane (τ,θ-plane)
			Closed Form	Integral Representation	Integral Representation
I	Non-lifting Circular Cyl. (Ref.2,3,5)	$w = z + \frac{1}{z}$. (T-I.1)	$w = (1-\zeta)^{-1/2} + (1-\zeta)^{1/2}$ (T-I.2)	$w = \frac{1}{2\pi i}\int_{-i\infty}^{i\infty} G_1(\nu)(-\zeta)^\nu d\nu$. (T-I.3)	$W = \frac{1}{2\pi i}\int_{-i\infty}^{i\infty} G_1(\nu)e^{-\nu s_1}\psi_\nu(\tau)(-1)^\nu e^{-i\nu\theta}d\nu$ (T-I.4)
II	Non-lifting Elliptic Cylinder (Ref.6)	$w = z' + \frac{1}{z'}$, $z = z' + \frac{\varepsilon}{z'}$. (T-II.1)	$w = \frac{2-(1+\varepsilon)\zeta}{\{(1-\varepsilon\zeta)(1-\zeta)\}^{1/2}}$ (T-II.2)	$w = \frac{1}{2\pi i}\int_{-i\infty}^{i\infty} G_2(\nu)(-\zeta)^\nu d\nu$. (T-II.3)	$W = \frac{1}{2\pi i}\int_{-i\infty}^{i\infty} G_2(\nu)e^{-\nu s_1}\psi_\nu(\tau)(-1)^\nu e^{-i\nu\theta}d\nu$. (T-II.4)
III	Lifting Circular Cylinder (Ref.2,4,5)	$w = z + \frac{1}{z} + \frac{i\Gamma}{2\pi}\log z$. (T-III.1)	$w = P+Q$, $P = \frac{i\Gamma}{4\pi}\{1 - \frac{1}{1-\zeta} - \log(1-\zeta)\}$, $Q = (1+\frac{1}{1-\zeta})\{1-\frac{\Gamma^2}{16\pi^2}-\zeta\}^{1/2} + \frac{\Gamma}{2\pi}\sin^{-1}[\frac{\Gamma/4\pi}{(1-\zeta)^{1/2}}]$. (T-III.2)	$w = P+Q$, $P = \frac{1}{2\pi i}\int_{-i\infty}^{i\infty} G_3(\nu)(-\zeta)^\nu d\nu$, $Q = \frac{1}{2\pi i}\int_{-i\infty}^{i\infty} G_4(\nu)(-\zeta)^\nu d\nu$. (T-III.3)	$W = \tilde{P}+\tilde{Q}$, $\tilde{P} = \frac{1}{2\pi i}\int_{-i\infty}^{i\infty} G_3(\nu)\frac{\psi_{-\nu}(\tau_1)+2\tau_1\psi'_{-\nu}(\tau_1)}{1-\nu}\psi_\nu(\tau)(-1)^\nu e^{-i\nu\theta}d\nu$, $\tilde{Q} = \frac{1}{2\pi i}\int_{-i\infty}^{i\infty} G_4(\nu)\frac{\psi_{-\nu}(\tau_1)+2\tau_1\psi'_{-\nu}(\tau_1)}{1-\nu}\psi_\nu(\tau)(-1)^\nu e^{-i\nu\theta}d\nu$. (T-III.4)
IV	Lifting Elliptic Cylinder (Ref.8)	$w = z' + \frac{1}{z'} + \frac{i\Gamma}{2\pi}\log z'$, $z = z' + \frac{\varepsilon}{z'}$. (T-IV.1)	$w = -\frac{i\Gamma}{4\pi}\{1 - \frac{(1-\varepsilon)\zeta}{(1-\varepsilon\zeta)(1-\zeta)} - \log\frac{1-\varepsilon\zeta}{1-\zeta}\} + \frac{2-(1+\varepsilon)\zeta}{\{(1-\varepsilon\zeta)(1-\zeta)\}^{1/2}}\{1-\frac{\Gamma^2/16\pi^2}{(1-\varepsilon\zeta)(1-\zeta)}\}^{1/2} + \frac{\Gamma}{2\pi}\sin^{-1}[\frac{\Gamma/4\pi}{\{(1-\varepsilon\zeta)(1-\zeta)\}^{1/2}}]$. (T-IV.2)	... ...	... ... $\frac{\psi_{-\nu}(\tau_1)+2\tau_1\psi_{-\nu}(\tau_1)}{1-\nu}$ is used throughout
V	Lifting Circular Cylinder + Additional Non-lifting Flow-function (Present Theory; Ref.9)		$w = P+Q$ (ibid. T-III.2) $-\{(1-\zeta/\zeta_2)^{-1/2}+(1-\zeta/\zeta_2)^{1/2}\} + \frac{1}{(1-\varepsilon)^{1/2}}\frac{2-(1+\varepsilon)\zeta/\zeta_2}{\{(1-\frac{\varepsilon\zeta}{\zeta_2})(1-\frac{\zeta}{\zeta_2})\}^{1/2}}$ * (T-V.2)	$w = P+Q$ (ibid. T-III.3) $-\frac{1}{2\pi i}\int_{-i\infty}^{i\infty} G_1(\nu)(\frac{-\zeta}{\zeta_2})^\nu d\nu + \frac{1}{2\pi i}\int_{-i\infty}^{i\infty}\frac{1}{(1-\varepsilon)^{1/2}} G_2(\nu)(\frac{-\zeta}{\zeta_2})^\nu d\nu$. (T-V.3)	$W = \tilde{P}+\tilde{Q}$ (ibid. T-III.4) $-\frac{1}{2\pi i}\int_{-i\infty}^{i\infty} G_1(\nu)\zeta_2^{-\nu}e^{-\nu s_1}\psi_\nu(\tau)(-1)^\nu e^{-i\nu\theta}d\nu + \frac{1}{2\pi i}\int_{-i\infty}^{i\infty}\frac{\zeta_2^{-\nu}}{(1-\varepsilon)^{1/2}} G_2(\nu)e^{-\nu s_1}\psi_\nu(\tau)(-1)^\nu e^{-i\nu\theta}d\nu$. (T-V.4)

$$G_1(\nu) = \frac{(\nu-1)(-\nu-1)!(\nu-3/2)!}{(-1/2)!},$$

$$G_2(\nu) = 2\frac{(-\nu-1)!(\nu-1/2)!}{(-1/2)!}F(\tfrac{1}{2}, -\nu; -\nu+\tfrac{1}{2}; \varepsilon) + (1+\varepsilon)\frac{(-\nu)!(\nu-3/2)!}{(-1/2)!}F(\tfrac{1}{2}, -\nu+1; -\nu+\tfrac{3}{2}; \varepsilon)$$
$$+2\varepsilon^{\nu+1/2}\nu!\frac{(-\nu-3/2)!}{(-1/2)!}F(\tfrac{1}{2}, \nu+1; \nu+\tfrac{3}{2}; \varepsilon) + \varepsilon^{\nu-1/2}(1+\varepsilon)\frac{(\nu-1)!(-\nu-1/2)!}{(-1/2)!}F(\tfrac{1}{2}, \nu; \nu+\tfrac{1}{2}; \varepsilon),$$

$$G_3(\nu) = \frac{i\Gamma}{4\pi}\frac{\pi}{\sin\pi\nu}\left(\frac{\nu-1}{\nu}\right), \qquad G_4(\nu) = \frac{(\nu-1)(-\nu-1)!(\nu-3/2)!}{(-1/2)!}F(\nu-\tfrac{1}{2}, -\tfrac{1}{2}; \tfrac{1}{2}; \tfrac{\Gamma^2}{16\pi^2}).$$

* The identity: $\zeta_2 \equiv 1 - (\frac{\Gamma}{4\pi})^2$ is used in this Table.

leading-edge. With these supplements to the classical theory, he was successful in obtaining the flow past obstacles which, after the compressible transformation, looked like realistic aerofoil sections, lifting and non-lifting.

Taking into consideration of the fact that Nieuwland's procedure would impose us too much labour for the numerical computation of a lifting aerofoil, we now make what is in a sense a fresh start, taking the following function as the generating (incompressible-flow) function. In a similar way as that has given sometimes fruitful results in the tradition of the classical aerofoil theory, we take as the basis the simplest flow: the flow past a (lifting) circular cylinder. We then intend to modify it by means of superposition of other flows, which would result in an effective measure of varying the final shape of the profile.

We assume the form:

$$w(\zeta)= w^{(0)}(\zeta) +w_1^{(A)}(\zeta) +w_2^{(A)}(\zeta), \qquad (10)$$

where

$$w^{(0)}(\zeta)= \frac{i\Gamma}{4\pi}\{1- \frac{1}{1-\zeta} -\log(1-\zeta)\}$$

$$+\frac{i\Gamma}{4\pi} \{(1+ \frac{1}{1-\zeta})(\frac{\zeta_2-\zeta}{\zeta_2-1})^{1/2} -\int_\infty^\zeta \frac{1}{1-\zeta}(\frac{\zeta_2-1}{\zeta_2-\zeta})^{1/2} d\zeta \} \qquad (11)$$

Hereafter, in this paper, we put

$$\zeta_2 = 1-(\Gamma/4\pi)^2, \quad (0<|\zeta_2|<1) \qquad (12)$$

for the sake of simplicity; then Eq. 11 reduces to Eq. T-III.2, and $w^{(0)}(\zeta)$ is exactly the flow past a lifting circular cylinder. At a later stage, however, another possibility will be considered in which ζ_2 is extended to be a complex number (see Section 2.4).

Meanwhile, for $w_1^{(A)}$ and $w_2^{(A)}$ are chosen the following functions as a first attempt:

$$w_1^{(A)} = -\{(1-\zeta/\zeta_2)^{-1/2} +(1-\zeta/\zeta_2)^{1/2}\}, \qquad (13)$$

$$w_2^{(A)} = \frac{1}{(1-\varepsilon)^{1/2}} \frac{2-(1+\varepsilon)\zeta/\zeta_2}{\{(1-\zeta/\zeta_2)(1-\varepsilon\zeta/\zeta_2)\}^{1/2}} \qquad (14)$$

where $\varepsilon =\varepsilon_0 e^{i\delta}$, and ε_0 and δ are real parameters, and $0 \leqq \varepsilon_0 < 1$.

It will easily be seen that $w_1^{(A)}$ takes the form of the flow past a non-lifting circular cylinder, the sign reversed and the branch point shifted from $\zeta=1$ to $\zeta=\zeta_2$. In a similar manner, $w_2^{(A)}$ is taken to be a flow past a non-lifting elliptic cylinder, with the branch point originally at $\zeta=1$ being shifted to $\zeta=\zeta_2$. Hence, each of them possesses a first-order branch point at the point $\zeta=\zeta_2$ in common with $w^{(0)}$; and a certain singularity (similar to that at $\zeta=1$ of Eq. 8) of $w_1^{(A)}$ and $w_2^{(A)}$ at $\zeta=\zeta_2$ cancelling each other, $w_1^{(A)} + w_2^{(A)}$ does not diverge at $\zeta=\zeta_2$.

Now, let us examine what kind of (incompressible) flow the function $w =w^{(0)} +w_1^{(A)} +w_2^{(A)}$ does represent.

(i) If $\varepsilon=0$, then $w_1^{(A)} + w_2^{(A)}$ vanishes; hence w ($=w^{(0)}$) naturally represent a flow past a circular cylinder with circulation.

(ii) If $\delta=0$ and $\Gamma=0$, then $\zeta_2=1$, and $w^{(0)} +w_1^{(A)}$ vanishes in turn; hence

$$w\ (=w_2^{(A)})= \frac{1}{(1-\varepsilon_0)^{1/2}} \frac{2-(1+\varepsilon_0)\zeta}{\{(1-\zeta)(1-\varepsilon_0\zeta)\}^{1/2}}, \qquad (15)$$

and this represents exactly a flow past a non-lifting elliptic cylinder with the eccentricity ε_0, the length of its major and minor semi-axis being $2(1-\varepsilon_0)^{-1/2}(1+\varepsilon_0)$ and $2(1-\varepsilon_0)^{-1/2}(1-\varepsilon_0)$, respectively.

(iii) If $\delta=0$, $\varepsilon\neq0$ and $\Gamma\neq0$, then w represents a flow past a body of fore- and- aft symmetry, resembling closely an elliptic cylinder, provided that Γ is small(see Fig. 1).

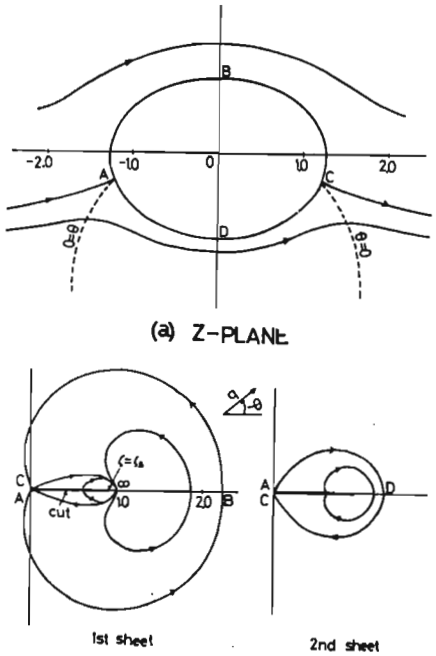

Fig.1. Incompressible flow past a pseudo-elliptical body: $\varepsilon_0=0.13$, $\Gamma=4.0$, $\delta=0.0$.

(iv) If $\delta\neq0$, then w does not represent an incompressible flow past any closed body. As will be seen later (Section 2.4), however, the parameter δ plays an important role in making the body closed in the compressible flow.

The integral representation of $w^{(0)}$, $w_1^{(A)}$, and $w_2^{(A)}$ is given in Table 1 (Eq. T-V.3); the paths of integration are not shown in this paper (see Ref.9). We constructed thus an artificial flow $w(\zeta)$ by superposition of 'ready-made' flow functions $w^{(0)}$, $w_1^{(A)}$, and $w_2^{(A)}$. The advantage of such a combination will in due course be verified.

2.3 The Incompressible-to-Compressible Transformation

We are going to transform the above (generating) function to that of the compressible flow, following the procedure described in Section 2.1. First we have to determine the functional form of the compressibility factor $f_v(\tau_1)$ to be used.

The simplest function which satisfies the conditions (see Section 2.1) imposed on $f_\nu(\tau_1)$ is

$$f_\nu(\tau_1) = e^{-\nu s_1} \tag{16}$$

However, we should not use this for the transformation of $w^{(0)}$, because the stream function $\Psi^{(0)}$ obtained in this way would have such an unacceptable behaviour that it would not recover its original value when the singular point $\tau=\tau_1$, $\theta=0$ is encircled once. This multivalence is caused by the singularity of $w^{(0)}$ expressed in Eq. 9. It has been demonstrated originally by Lighthill[2,4] that, in order to avoid this difficulty, we should use

$$f_\nu(\tau_1) = \frac{\psi_{-\nu}(\tau_1) + 2\tau_1\psi'_{-\nu}(\tau_1)}{1-\nu} \tag{17}$$

for a flow with circulation like $w^{(0)}$. (The prime in the above expression denotes the differentiation with respect to τ.)

In contrast to that, we are justified to apply Eq. 16 to $w_1^{(A)}$ and $w_2^{(A)}$ because they, representing flows without circulation, do not suffer from such singularity.

Hence, the compressible-flow function corresponding to Eq. 10 is given as W described in Eq.T-V.4 of Table 1. (The statement on the paths of integration is omitted again.) It should be noted that, in contrast to $e^{-\nu s_1}$ which has no pole all over the ν-plane, $\{\psi_{-\nu}(\tau_1)+2\tau_1\psi'_{-\nu}(\tau_1)\}/(1-\nu)$ has simple poles at $\nu = 1, 2, 3, \cdots$; therefore the integrands of the first two integrals in Eq.T-V.4 (which are the same as those in Eq.T-III.4) come to have double poles at $\nu=2, 3, 4, \cdots$, and also quite a detrimental simple pole at $\nu=1$ which will be discussed later in this Section.

At all events, the integrals in Eq.T-V.4 can be evaluated by way of the residue theorem to yield a set of infinite series involving Chaplygin's particular solutions (2). The solution W in (τ,θ) plane has several singular points corresponding to those of w in ζ-plane [e.g. $(\tau_1,0)$ corresponding to $\zeta=1$; $(\tau_2,0)$ to $\zeta=\zeta_2$]. It follows that each series solution has a specific region of convergence, and the evaluation of the integral solutions by way of series expansion must be performed separately at each region of convergence. (The process of this evaluation will not be presented here; see Ref.9 for the detail.)

Once the stream function Ψ has been established in series form on the hodograph plane, it is not difficult to obtain its transformation onto the Z (physical) plane from the following equations (derived from the basic hodograph equation and the definition of the stream function):

$$\frac{\partial Z}{\partial\theta} = \left(\frac{\tau_1}{\tau}\right)^{1/2} \frac{2\tau}{(1-\tau)^{1/(\gamma-1)}} e^{i\theta}\left\{\frac{\partial\Psi}{\partial\tau} + \frac{i}{2\tau}\frac{\partial\Psi}{\partial\theta}\right\}$$

$$\frac{\partial Z}{\partial\tau} = \left(\frac{\tau_1}{\tau}\right)^{1/2} \frac{2\tau}{(1-\tau)^{1/(\gamma-1)}} e^{i\theta}\left\{\frac{i}{2\tau}\frac{\partial\Psi}{\partial\tau} - \frac{1-\frac{\gamma+1}{\gamma-1}\tau}{4\tau^2(1-\tau)}\frac{\partial\Psi}{\partial\theta}\right\} \tag{18}$$

Now, the compressible-flow solution is formally determined. In the case of a flow with circulation, however, the series solutions expressing the flow near both stagnation points ($\tau=0$) contain terms of the form $\psi_1(\tau)e^{-i\theta}$ which come from the residue of the pole at $\nu=1$ of $f_\nu(\tau_1)$ in Eq.17; consequently the position coordinates in the physical plane become logarithmically infinite for $\tau\to0$, and the closure of the body contour (i.e. the streamline $\Psi=0$) breaks down as far as the free-stream Mach number is not equal to zero.

Therefore, we have to take some measure in order firstly to obtain a flow with a regular stagnation point at the front of the contour. (The problem of getting the contour closed at the rear will be discussed in Section 2.4.) It has been recommended[5,8] for this purpose to subtract the detrimental terms cited above (and also other inessential terms), which appear in the region covering front stagnation point, from the series solution for this region as well as from those for all other regions. As these terms themselves make solutions of the basic equation, this manipulation is permissible as far as these terms are convergent in all regions.

After all, we have the series solution modified as follows. (Only the solution in the neighbourhood of the front stagnation point is shown in this paper.)

$$\Psi = \mathrm{Im.}\,[K^{(0)}+K_1^{(A)}+K_2^{(A)}], \tag{19}$$

$$K^{(0)} = \sum_{n=2}^{\infty} C_n \frac{\psi_n^*(\tau_1)+2\tau_1\psi_n^{*\prime}(\tau_1)}{1-n}\psi_n(\tau)e^{-in\theta}, \tag{20}$$

$$K_1^{(A)} = \sum_{n=2}^{\infty} B_n\, e^{-ns_1}\,\psi_n(\tau)e^{-in\theta}, \tag{21}$$

$$K_2^{(A)} = \sum_{n=2}^{\infty} D_n\, e^{-ns_1}\,\psi_n(\tau)e^{-in\theta}, \tag{22}$$

where $\psi_n^*(\tau)$ denotes the Chaplygin function of the second kind -(note that $\psi_n(\tau)$ of Eq. 3 hitherto used is the Chaplygin function of the first kind)- defined as

$$\psi_n^*(\tau) = \lim_{\nu\to-n}\frac{\partial}{\partial\nu}(\nu+n)\psi_\nu(\tau), \qquad n=2, 3, 4, \cdots \tag{23}$$

and C_n, B_n, D_n are the coefficients of the Taylor series when $w^{(0)}(\zeta)$, $w_1^{(A)}(\zeta)$, and $w_2^{(A)}(\zeta)$, respectively, are expanded in the neighbourhood of the front stagnation point, i.e.

$$C_n = \frac{(1-n)(n-3/2)!}{(-1/2)!\;n!}\,F\left(n-\frac{1}{2},\,-\frac{1}{2};\,\frac{1}{2};\,\frac{\Gamma^2}{16\pi^2}\right) + \frac{i\Gamma}{4\pi}\left(\frac{1}{n}-1\right), \tag{24}$$

$$B_n = \zeta_2^{-n}\,\frac{(n-1)(n-3/2)!}{(-1/2)!\;n!}, \tag{25}$$

$$D_n = \frac{-\zeta_2^{-n}}{(1-\epsilon)^{1/2}}\left\{\frac{2(n-1/2)!}{(-1/2)!\,n\,!}F\left(\frac{1}{2},\,-n;\,-n+\frac{1}{2};\,\epsilon\right) -(1+\epsilon)\frac{(n-3/2)!}{(-1/2)!(n-1)!}F\left(\frac{1}{2},\,-n+1;\,-n+\frac{3}{2};\,\epsilon\right)\right\} \tag{26}$$

2.4 Additional Techniques for Obtaining Aerofoil Sections

In addition to the fundamental procedure described in the previous sections, we have to establish other ad. hoc. techniques in order to obtain a flow past an aerofoil section.

The solution Eq. 19 yields certainly a flow with a front stagnation point as far as the free-stream Mach number M_1 is restricted within small values (i.e. τ_1 is small). As M_1 increases, however, the leading-edge radius becomes smaller and smaller. If we take an example of non-lifting symmetrical flow ($\Gamma=0$ and $\delta=0$) for a large value of ε_0, the leading-edge degenerates into a cusp beyond a certain Mach number M_1, though the profile still keeps a closed contour at both edges (see Fig. 2). The situation becomes much worse in the lifting case, in which we should expect that the contour might fail to close up even at the front.

Here we try to superpose on Eq. 19 another series equation $\mathrm{Im}.[\lambda L]$, which is convergent for $0\leqq\tau<1$ and tends to zero as $M_1\to 0$, in the expectation that a moderate amount of the leading-edge radius would be thereby maintained at higher Mach numbers. Eq.19 is hence revised again to yield

$$\Psi = \mathrm{Im}.[K^{(0)}+K_1^{(A)}+K_2^{(A)}+\lambda L], \tag{27}$$

where λ is a real parameter. The function L is the familiar series solution which comes out when one executes the analytic continuation of $K_2^{(A)}$ (the flow past a non-lifting elliptic cylinder) encircling once round the branch point $\tau=\tau_2,\theta=0$, and defined as:

$$L = \sum_{n=2}^{\infty} E_n\left\{\frac{-n(a_n-1)!(n-b_n)!}{(a_n-n-1)!(-b_n)!(n!)^2}\right\} e^{ns}\psi_n(\tau)e^{in\theta} \tag{28}$$

where

$$E_n = \frac{-\zeta_2^n}{(1-\varepsilon)^{1/2}}\left\{\frac{2\pi(n-1)!}{(-1/2)!(n-1/2)!}F\left(\frac{1}{2},\ n;\ n+\frac{1}{2};\ \varepsilon\right)\right.$$
$$\left.-(1+\varepsilon)\frac{\pi n!}{(-1/2)!(n+1/2)!}F\left(\frac{1}{2},\ n+1;\ n+\frac{3}{2};\ \varepsilon\right)\right\} \tag{29}$$

This is a technique quite similar to that used for the same purpose in Nieuwland's theory[6] for a non-lifting elliptic cylinder. He then built up a solution which in our notation would be expressed as:

$$\Psi = \mathrm{Im}.[K_2^{(A)}+\lambda L]\ ; \tag{30}$$

and he investigated the effect of the second term λL, which showed a marked effect in controlling the leading-edge radius of the resulting aerofoil. Coming back to the solution (27), we notice by actual computation that the term λL still works as an effective element controlling the leading-edge radius R_0 for both non-lifting and lifting cases. An example of symmetrical profile with a finite leading-edge radius obtained by (27) is shown in Fig.3.

Having settled the problem of the leading-edge radius, we now face to the last difficulty concerning the closure of the trailing-edge, which is not yet ensured in the lifting-aerofoil case. It can be seen from the computation of the flow by the procedure developed so far that there exists a saddle point at a certain point S on one sheet of the hodograph plane, where $\partial\Psi/\partial\theta=\partial\Psi/\partial\tau=0$. The saddle point corresponds to a first-order branch point on the physical (Z-)plane, and the above fact implies that Z-plane is also constituted of two sheets of the Riemann surface. Bearing in mind the assembly of streamlines on the hodograph plane, we notice that there must be one streamline that will pass the saddle point S. Assume that it is the streamline $\Psi=c$, say. Then two branches of $\Psi=c$ meet at S on the hodograph plane; on the physical plane, two branches of the mapped streamline $\Psi=c$ would certainly cusp at the branch point corresponding to S. As to any other streamline ($\Psi\neq c$) which does not pass the saddle point S on the hodograph plane, one branch of its image on Z-plane goes to infinity on the first sheet while the other branch passes into the second sheet; and they will never meet again. The latter situation generally occurs for the streamline $\Psi=0$ that would build up the contour of an aerofoil; it follows that the profile does not close up at the rear end. Only

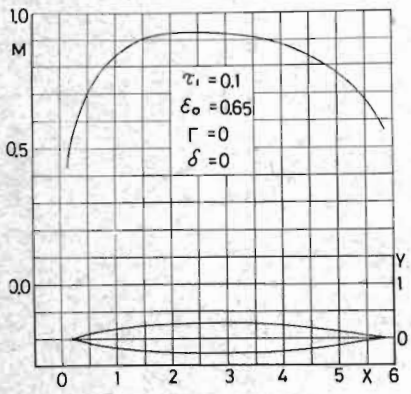

Fig. 2. Symmetrical section with cusped leading and trailing edges.

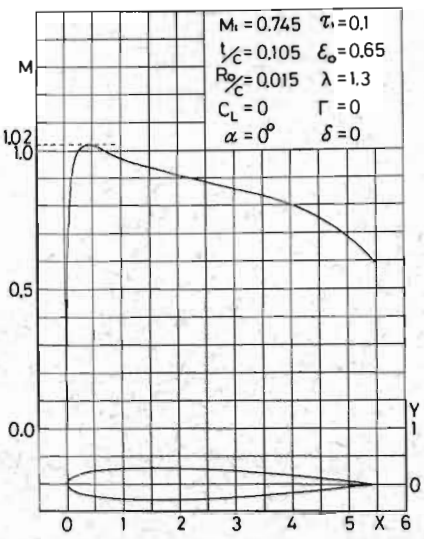

Fig. 3. Symmetrical section with a blunt leading edge.

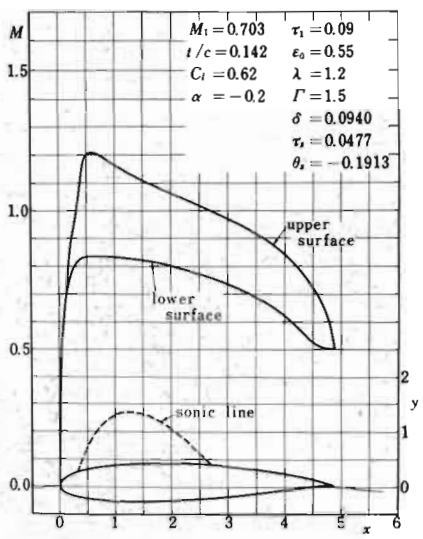

Fig. 4. An example of lifting aerofoil section. (7062-14)

if, by any chance, $\Psi=0$ be the proper streamline that passes the saddle point S on the hodograph plane, we would have a closed profile with a cusped trailing-edge.

If we want a closed profile in general cases, we have to take a device by means of which Ψ will satisfy the condition

$$\frac{\partial\Psi}{\partial\theta} = \frac{\partial\Psi}{\partial\tau} = \Psi = 0 \qquad (31)$$

simultaneously at a point S on the hodograph plane. Due to such device, the local condition of the flow must naturally be modified since the contour becomes now closed by its application; it is desirable, however, that it would not so much modify the general aspects of the original fow configuration. There are various possibilities for such device.

(i) One of them is to superpose to the present solution still other supplementary solutions with arbitrary constant factors. These factors are determined in such a manner that Ψ in total would satisfy the condition (31) at the point S. This is the technique used by Nieuwland[8], and we followed this process at an early stage of the computation.

(ii) Attention is now called to the fact that we have another arbitrary parameter δ at hand (see the comment in (iv), Section 2.2). The whole flow field Ψ undergoes a gradual change with variable δ. Hence, by proper choice of the value of δ we can satisfy the condition (31) at a certain point on the hodograph plane with pre-determined values of $\tau_1, \varepsilon_0, \lambda$, and Γ ; the saddle point (τ_s, θ_s) hereby being submitted to a slight deviation from its original location at $\delta=0$. As the increment of Ψ due to δ is shown to be of the order

$$2\varepsilon_0(1-\varepsilon_0)^{-3/2}\,\delta \qquad (\text{if } |\delta| \ll 1)$$

at the rear part of the aerofoil, we can estimate from this the approximate value of δ by which Eq. 31 becomes satisfied.

(iii) Finally, another device is to release ζ_2 from the fixed real-value $1-\Gamma^2/16\pi^2$, and extend it into the domain of complex numbers. That will provide us even other arbitrary parameters.

If we use the devices (ii) and (iii) jointly, we can satisfy the condition (31) at a specified saddle point (τ_s, θ_s). The conversion from the device (i) to this is under way in our system of computation.

2.5 Discussion to the Present Theory

Reviewing the present theory, we emphasize that twofold simplication is hereby achieved in respect of numerical computation. Firstly, the series solution for W in the present theory is expressed by only doubly-infinite series. (See Eqs.19~22, for instance, in which the coefficients C_n etc. are regarded as (singly-infinite) series because they include hypergeometric functions: see Eq. 24 etc.) On the other hand, if we start from an incompressible flow past a lifting elliptic cylinder (CASE IV in Table 1), we should have to deal with triply-infinite series since the coefficients themselves would make doubly-infinite series. The reduction from a triple to a double series saves a great deal the labour of numerical computation. Note that it results from the particularly simple form of the original flow function used in this theory. Secondly, as was mentioned in Section 2.3, the simplest form $e^{-\nu s_1}$ of $f_\nu(\tau_1)$ can be used for $W_1^{(A)}$ and $W_2^{(A)}$; the use of $e^{-\nu s_1}$ which has no pole in the ν-plane turns out to eliminate the appearance of double poles at $\nu = 2, 3, 4, \cdots$ in the integrand, and hence serves in reducing considerably the number of series to be computed.

Various lifting profiles with shock-free mixed-flows have been computed by the present method. Typical examples are shown in Figs. 4, 5, and 6. A feature of profiles of this particular family is well shown by the shape of the profiles and the local Mach-number distribution. Each of them has a mild

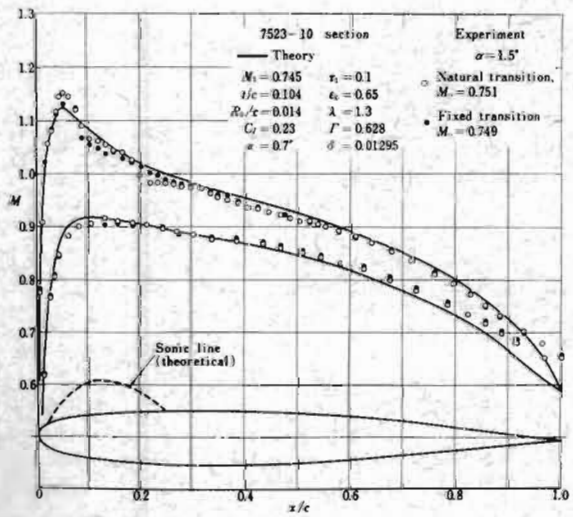

Fig. 5. Profile shape and local Mach-number distribution of the 7523-10 section. Comparison between the test result and the theory.

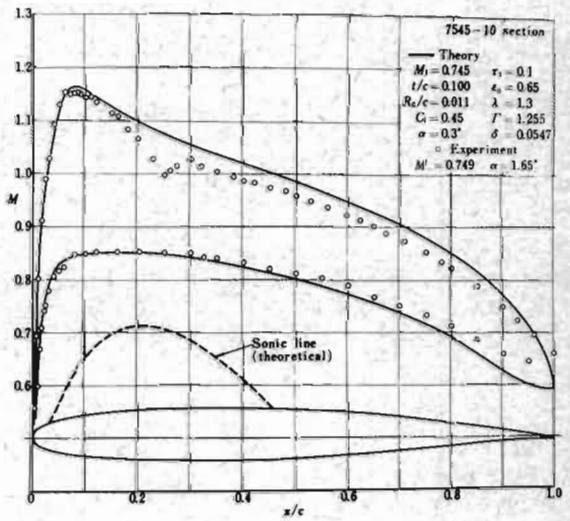

Fig. 6. Profile shape and local Mach-number distribution of the 7545-10 section. Comparison between the test result and the theory.

suction peak just downstream of the leading-edge, and a certain amount of camber distributed all over the chord length. The impression of such features of profiles is that they lie intermediate between NLR's lifting aerofoil[10] and that of Garabedian-Korn's[11].

After all, the shape and characteristics of each profile calculated by this method are determined by several parameters; $\tau_1, \varepsilon_0, \lambda$, and Γ being the essential ones. If δ and complex ζ_2 are included, the number of parameters would further increase as long as they are not consumed during the process of getting the profile closed. Such number of arbitrary parameters would be sufficient to represent the gross feature of the flow past a specific aerofoil section. To modify the local conditions, however, additional scheme would perhaps be useful. In consideration of the fact that the original flow-function used in this theory is a composition of those for circular and elliptic cylinders (in which the branch-point singularities in the hodograph plane dominate in characterizing the features of the profile), a theory for the flow with additional logarithmic singularities, located inside of the body, is being developed now.

3. Experimental Verification of the Pressure Distribution of Aerofoils Obtained by Exact Theory

After the completion of the theory described in Section 2, we went ahead, as a matter of course, with wind-tunnel tests of some of the profiles obtained, and particularly aimed at the experimental verification of the (shock-free) pressure distribution on the wing surface[12]. The wind tunnel used was 2m.x 2m. Transonic Tunnel in NAL; the Reynolds number, based on the chord-length of 400 mm., ranged $3.85 \sim 5.5 \times 10^6$ depending on Mach numbers.

3.1 7523-10 Section

This is a profile obtained at an early stage of computation. It is of 10.4% thickness and designed for M_∞ ($\equiv M_1$ in the theory)=0.745 and C_l=0.23 (see Fig.5). The distribution shows a mild peak at about 5% chord point on the upper surface, and the local Mach number of 1.12 is attained there.

The model (of 2m.-span and 400mm.-chord) was located at the centre of the test-section, spanning the whole test-section width from a side-wall to the other, and supported at both tips by a pair of metal arms which passed through the slots of glass-windows and were fixed to the outer frame of the test-section.

Originally, the test-section of this tunnel had been equipped with perforated walls of 20% open-area ratio on the four sides. As this particular test was of two-dimentional in nature, both side-walls were covered from the outside of the test-section with aluminium plates of 3mm.-thickness close to the original wall-plates, and they worked practically as solid walls. The top- and bottom-walls maintained their original configuration.

The pressure distribution was measured by pressure orifices drilled at the mid-span section and also the quarter-span section (500mm. apart from the mid-span section)of the model; a pitot-rake situated at one chord-length downstream of the trailing-edge was used for the wake survey. Tests were performed mostly with natural transition on

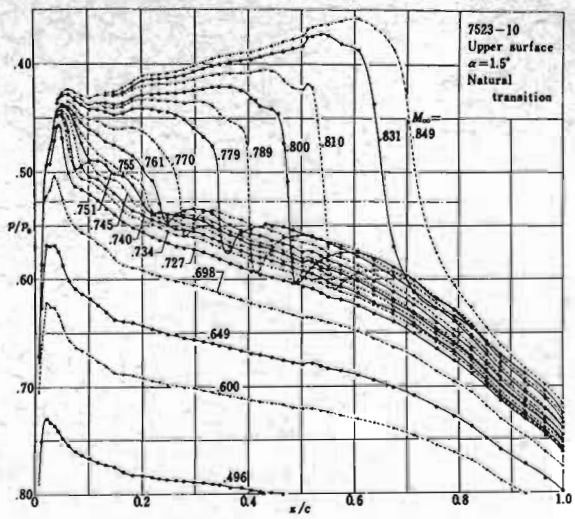

Fig. 7a. The upper-surface pressure distribution of the 7523-10 section at α= 1.5°. Natural transition.

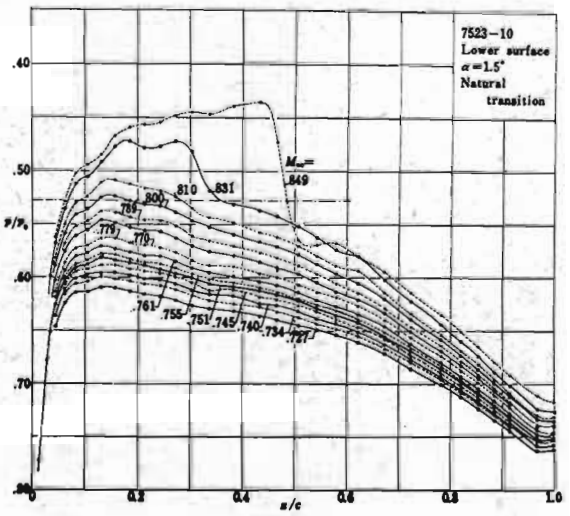

Fig. 7b. The lower-surface pressure distribution of the 7523-10 section at =1.5°. Natural transition.

the model, but tests with fixed transition as well as tests with varied open-area ratio (of the top- and bottom-wall)were also performed at a later stage.

It became clear at the first test that the measured pressure distribution at the design point (M_∞ =0.745, α =0.7°) did not show the best agreement with the theoretical distribution. The reason of the discrepancy was considered to be:

(i) The boundary layer effect, which caused the modification of the effective body-shape (displacement effect) on the one hand, and also a certain loss of the lift, on the other.

(ii) The wind-tunnel wall interference was expected to be negligible in our initial, wishful thinking; but in fact it was not so. Ebihara et. al.[13]

performed several theoretical analyses and derived the subcritical characteristics of this profile, which could be regarded as interference-free values. (Their analyses included the linear theory and the boundary layer calculation which were only applicable to subcritical conditions.) They compared these values to the experimental results, and found that a wall-interference effect of considerable amount (corresponding to the change of the angle of attack of approximately 1° at this C_l level) seemed to exist in the test results even at such subcritical Mach numbers. There is no reason why the similar effect does not exist at supercritical conditions.

If a certain loss of lift occurs by some origin or other, it would certainly influence the position of the leading-edge stagnation point. That, in turn, will alter the process of expansion following the stagnation point (which is quite critical for the existence of a shock-free flow), and might spoil the whole flow field predicted by the theory.

The discrepancy would be reduced to some extent if we compensate for the defect of the lift by increasing the uniform-flow Mach number and/or the angle of attack. In fact we found that the best agreement with the theoretical pressure distribution could be attained at M_∞=0.751 and α=1.5° (Fig. 5): this happened to be one of the test conditions in which the position of the front stagnation point was very close to that obtained from the theory. Agreement of the lower-surface distribution is acceptable notwithstanding the difference in the flow condition between the theory and the test. Agreement of the upper-surface distribution is not bad, too, but we notice that the nose-peak Mach number is somewhat higher in the test data. We notice also that a slight over-compression follows as a result of the reflection, at the sonic line, of the above-mentioned over-expansion at the peak.

Fig.7 shows the pressure distribution over the profile at varied test Mach numbers,the angle of attack being fixed at 1.5°. At Mach numbers higher than 0.76, the shock wave gradually develops at the recompression region rear of the peak,and proceeds rearward as the Mach number increases. At Mach number below 0.75, we cannot identify the shock wave from the pressure-distribution curve; if it does exist,it must certainly be very weak,and difficult to distinguish from the isentropic compression following the peak.

Fig.8 shows the pressure distribution curves at various angles of attack with the Mach number fixed approximately at M_∞ =0.75. In a similar way to Fig. 7, shock waves are recognizable only at angles of attack higher than 1.6°. As is expected from these pressure-distribution curves, no pronounced 'drag creep' is noted at low Mach number level; the lift and the drag curves are shown in Fig.9.

By inspection of the distribution in the vicinity of the shock-wave position in Figs.7 and 8, it was almost evident that the boundary layer there was still laminar. There were also symptoms of a short bubble of laminar-separation at the steep recompression region after the peak. The boundary layer

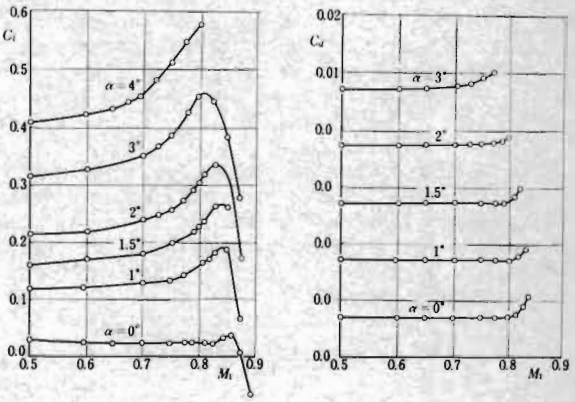

Fig. 9. The lift- and drag-coefficients of the 7523-10 section. Natural transition.

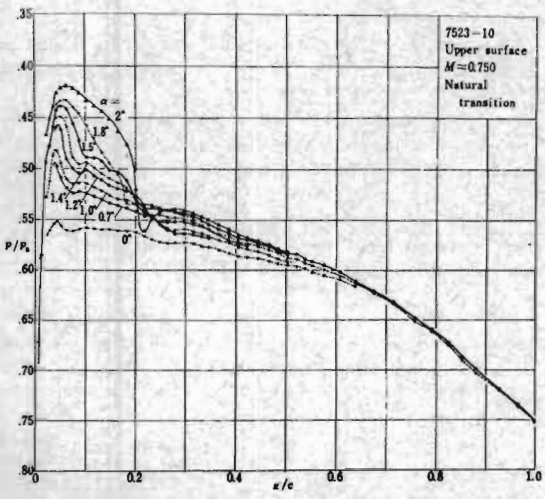

Fig. 8. The upper-surface pressure distribution of the 7523-10 section at M_∞=0.750. Natural transition.

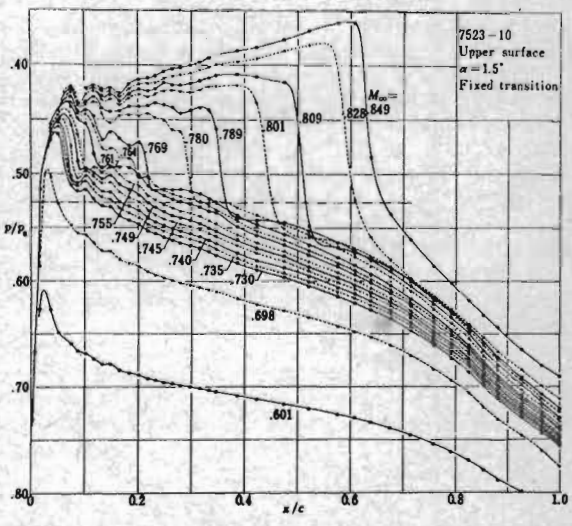

Fig. 10. The upper-surface pressure distribution of the 7523-10 section at α= 1.5°. Fixed transition. (cf. Fig. 7a.)

tripping technique was then applied with a roughness band consisting of glass beads of 0.08 mm. in diameter placed at 4~5% chord position from the leading-edge (upper surface). The pressure distribution at this fixed-transition condition revealed more reasonable features in predicting the flow condition at higher Reynolds numbers. However, the pressure distribution around the peak was somewhat disturbed by the roughness band (Fig.10). The tests at higher Reynolds numbers are most desirable in this respect.

3.2 7545-10 Section

This is a profile belonging to the same series as 7523-10 section, and isdesigned for the lift-coefficient C_l =0.45.

Tests of this wing were also performed in 2m. Transonic Tunnel, but with a model of 400mm. chord-length and 800mm. span. The model was set vertically 100mm. apart from the floor-wall, and fixed at one tip to the turn-table of the floor balance (an external balance). A pair of circular side-plates of 1m. in diameter were placed at both wing-tips and fixed independently to the wall, keeping small gaps to both wing-tips. The pressure distribution was always measured at the mid-span and the quarter-span sections; as they showed excellent agreement between them (except at the shock position where the pressure was submitted to a sudden change), the wing-tip effects were considered to be negligible and the flow to be uniform.

In various respects the characteristics of this wing section were like those of 7523-10 section. The agreement with the theoretical distribution was less satisfactory, possibly because the design lift-coefficient was higher. Only the 'best agreement' data is shown in Fig.6.

4. Other Lines of Investigation

Ever since the early stage of research on transonic aerofoils in NAL, empirical approach has been attempted independently from the fore-mentioned exact theory. The initial objective was to explore the section shape with a pronounced suction peak which was to generate a practically shock-free flow as proposed by Pearcey[1]; the later objective was to get a quick access to the design of aerofoil sections based on the new technology, without restriction imposed by an 'isentropic' flow which the exact theory principally concerned. We had a small two-dimentional, blowdown wind-tunnel (with a 100x400mm. test section) at hand, and most of the experimental works described in this Section were performed in this tunnel. The Reynolds number obtained was of the order 2×10^6 with a 100mm. chord wing model.

4.1 J. Sato[14], who had previously achieved an improvement of the existing inverse method in the incompressible flow theory, took advantage of his method and designed a number of profiles including those which were to generate a pronounced suction-peak in the scope of the incompressible-flow theory. Some of these profiles were tested at transonic Mach numbers, and the results were very much encouraging. An example of his profiles is shown in Fig.11. A series of these profiles were incorporated into a three-dimentional model (a wing-fuselage model with a swept and tapered wing) by the hand of the aircraft industry as an alternative proposal of the wing configuration of an aeroplane under development

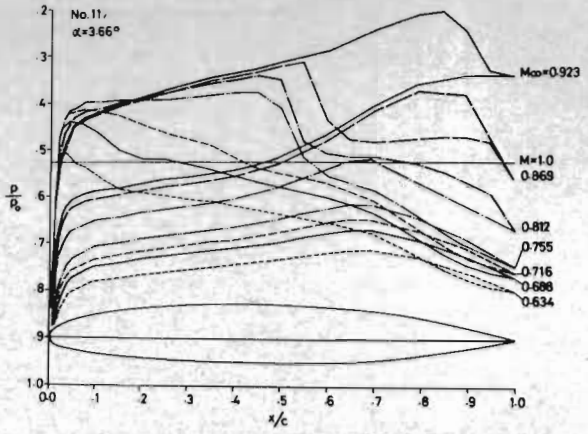

Fig. 11. The pressure distribution of the No. 117-3-173 section at α= 3.66°.

at that time. Results of the tests in the 2m. Transonic Tunnel showed a considerable improvement in the aerodynamic characteristics, at least in the transonic regime, of this new scheme compared with other configurations in use of conventional wing sections.

4.2 At a later period, N.Kamiya[15] tried to work out another procedure of designing transonic aerofoil sections.

He first reconfirms with ample experimental data the following, lately well-documented facts:

(i) Even if a wing section is in a supercritical flow condition, the pressure distribution over the subcritical parts on both surfaces of the wing can be well predicted from the low-speed pressure distribution by way of Prandtl-Glauert rule, for instance.

(ii) The pressure distribution along the supercritical part of the aerofoil is difficult to predict, and the Prandtl-Glauert rule, if applied, would give only a fictitious distribution there. However, as the pressure distribution of upper and lower surfaces is nearly independent from each other, and particularly so when the flow 'freezes' on one surface, it can be deduced that the supercritical distributions of two wing-sections at a same Mach number are at least the same if the shape (or equivalently the low-speed pressure distribution) of the upper surfaces of them are the same.

Kamiya further verifies experimentally that:

(iii) The supercritical distributions of two wing sections at different Mach numbers and possibly at different angles of attack are approximately the same if the versions of them in terms of Prandtl-Glauert rule (the fictitious distributions) at respective Mach numbers are the same.

Bearing these facts in mind, he concentrates on the drag-divergence problem of the wing section. He assumes that the superiority in respect of the drag-divergence characteristics (that means the drag-divergence Mach number M_{DD} is highest at a given C_l-value and a given thickness-ratio, for instance) of a wing section is well symbolized by the pattern of the pressure (p/p_0) distribution on the upper surface of that particular wing section at the drag-divergence condition. (Wing section generating a strong shock on the lower surface at

M_{DD} are temporally excluded from the consideration.) He selects a few examples from the pressure distribution data of the past, which did emerge under the seemingly excellent drag-divergence conditions. A criterion he adopts at the selection of the 'model' distribution is that it would provide the value of the integral

$$F = \int_0^c (p/p_0)_{DD}\, dx$$

over the wing upper surface as small as possible (i.e. the enclosed area of the upper-surface pressure-distribution curve as large as possible; c: the chord-length, x: the chordwise distance from the leading-edge, and the subscript DD denotes the drag-divergence condition).

He then posturates that, if approximately the same upper-surface pressure-distribution can be reproduced at the drag-divergence condition of another wing section subject possibly to different design criteria, the latter would also be a good wing section in respect of the drag-divergence characteristics. Thus he formulates the following procedure of designing a new profile which imitates the 'model' pressure distribution at different design conditions.

STEP 1. One of the model pressure distribution $\hat{p}/p_0$ he specifies tentatively is that of 780-450-12 section at the drag-divergence condition ($\hat{M}_\infty$=0.780, $\hat{C}_l$=0.45; the circumflex ^ denotes the 'model' condition). From the shape of this profile, one first calculate the incompressible pressure coefficient $\hat{C}_{p,I}$. Then, one applies to it the Prandtl-Glauert rule and derives the fictitious pressure distribution $(p/p_0)_{PG}$ at the Mach number $\hat{M}_\infty$.

STEP 2. The fictitious distribution $(p/p_0)_{PG}$ just obtained is regarded to be that of a new profile at a uniform-flow Mach number M_∞. The incompressible pressure-coefficient $C_{p,I}$ over the upper surface of the new profile is then obtained by the reversed process of the Prandtl-Glauert rule. In other words, $C_{p,I}$ is given by the following equation based on the definition of the pressure coefficient:

$$\frac{1}{p_0}\left(p_\infty + q\,\frac{C_{p,I}}{\beta}\right) = \left(\frac{p}{p_0}\right)_{PG} = \frac{1}{p_0}\left(\hat{p}_\infty + \hat{q}\,\frac{\hat{C}_{p,I}}{\beta}\right)$$

where p_0, p_∞, and q are the total, static, and dynamic pressures, respectively, of the uniform flow, β is the Prandtl-Glauert factor $(1-M_\infty^2)^{1/2}$, and the total pressure p_0 is set equal at both conditions.

STEP 3. Let $C_{p,I}$ thus obtained be called as the 'reduced' $C_{p,I}$. From the reduced $C_{p,I}$ one can calculate easily the shape of the new profile (the inverse method is used). Sometimes, the reduced $C_{p,I}$ might have to be modified at the front peak in order to obtain a feasible value of the suction-peak pressure at M_∞; meanwhile, the reduced $C_{p,I}$ can be modified almost arbitrarily at any chordwise position where the subcritical flow is eventually to develop at the Mach number M_∞.

In Fig.12, some wing sections are shown, which have been developed from the model section 780-450-12. It is seen that they exhibit the pressure distribution on the upper surface like that of the model section. It is interesting to note that profiles of considerably high M_{DD} have been obtained by this procedure. An example is shown in Fig.13. In Fig.14 are plotted the M_{DD} values, versus C_l, of several wing sections developed so far by this method.

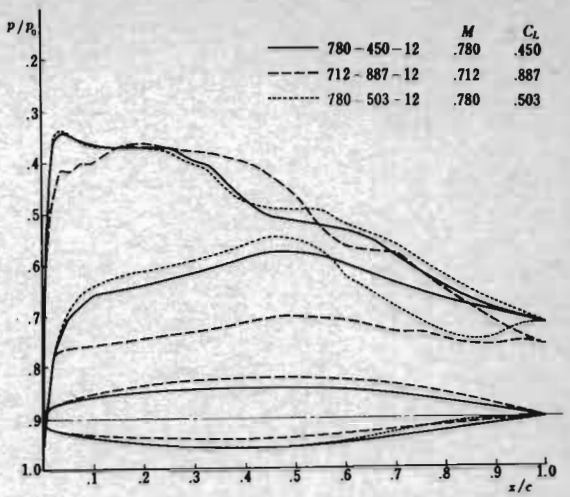

Fig. 12. Profile shape and the pressure distribution of the model section 780-450-12 and other sections derived from that.

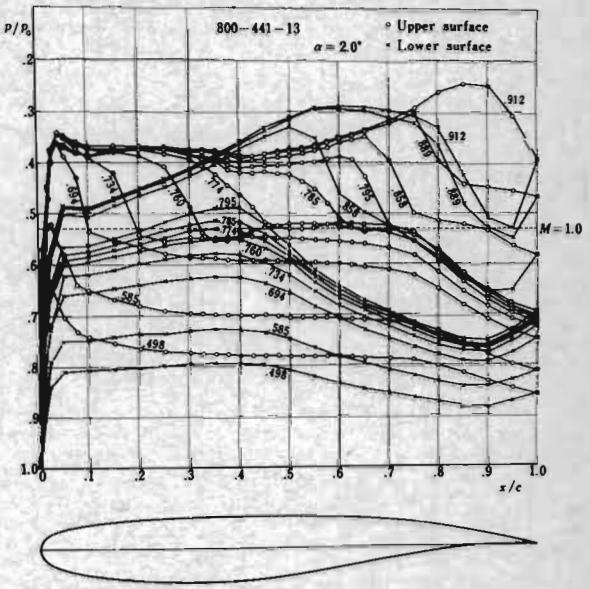

Fig. 13. Profile shape and pressure distribution of the 800-441-13 section at =2.0°.

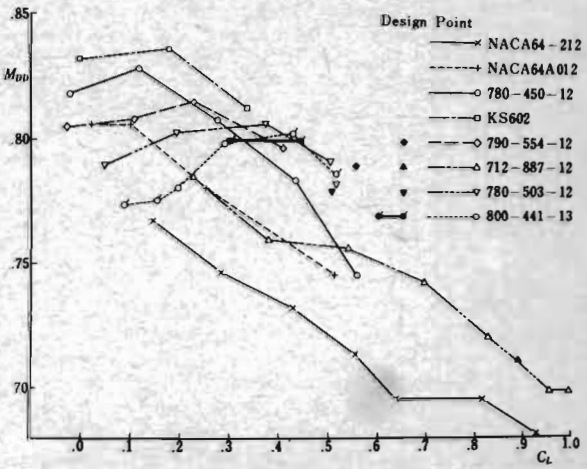

Fig. 14. Drag-divergence Mach number vs. lift coefficient of the newly developed wing sections compared with those of NACA 64-series sections.

5. Concluding Remarks

Since the time when the exact solution of the hodograph equation was successfully utilized in the investigation of the shock-free mixed-flow around an obstacle which was much like an aerofoil section in shape, this approach has been expected to make a powerful tool in the practical design problems. Nowadays there are several methods of computation based on the hodograph method, and families of aerofoil sections can be computed therefrom; practically shock-free flow on these profiles has been verified also by wind-tunnel tests. It cannot be denied, however, that,much of these profile-shapes have been determined according to the mathematical convenience rather than the physical requirement. If we seek an analogy in the history of classical aerofoil theory, we are in a situation as if we have just got possession of Joukowski aerofoils. It is most desirable that we could increase the number of computed profiles, and above all,design a wing section which answer to the physical or design requirements.

One notices from the experiment that the development of the flow on a (peaky-type) aerofoil, after the supercritical flow is first established at the peak, seems to be as follows.

(i) As far as the Mach number is not so much higher than the critical one, the flow comes back to the subsonic state by a severe recompression aft of the peak; and, in general cases, a portion of the recompression is effectuated by a shock wave, either weak or strong. If the shock wave is too strong, it would result in a high drag-level of the wing section at low Mach numbers (i.e. the drag creep).

(ii) As the Mach number goes up, the recompression aft of the peak comes to be more or less gradual for certain aerofoil sections. Under the most favourable condition it is constituted by the isentropic compression that the theory predicts. At still higher Mach numbers, the gradual recompression collapses; the supercritical flow, now forming a plateau of high-suction region, is finally terminated by a (terminal) shock which brings about the drag divergence.

(ii') For other wing sections, for which the leading-edge suction peak is too high and steep, the severe recompression which follows does not swich over to a gradual deceleration of the flow. Instead, the flow, after going down rapidly to the subsonic state, experiences again the expansion at the mid-chord position; that leads the flow afresh into the supercritical state accompanied by a terminal shock. (Sometimes a double-shock system is observed.) It is interesting to note that M_{DD} may sometimes be rather high in such cases. At higher Mach numbers, the intermediate subsonic region disappears; then occurs the formation of the plateau, and the final state of affairs is similar to that of the process (ii).

Taking account of the fact that the drag rise in a practical sense of a shock-free profile takes place at a considerably higher Mach number than that of the shock-free condition, and from the observation described above, we notice there are many interesting phenomena to be investigated at off-design conditions, which lie between the critical and the drag-divergence Mach numbers. It is most desirable that the existing methods of approach, including the direct method and the wind-tunnel test, will be fully utilized for the investigation of the flow phenomena comprehensive of these problems.

References

1. Pearcey, H.H.,'The aerodynamic design of section shapes for swept wings', Advances Aero. Sci., Vol.3, 1962.
2. Lighthill, M.J.,'The hodograph transformation in trans-sonic flow. III.Flow round a body', Proc. Roy. Soc., London, A 191, 1947.
3. Goldstein, S., Lighthill, M.J., and Craggs, J.W., 'On the hodograph transformation for high speed flow. I. A flow without circulation.' Quart. J. Mech. & Appl. Math. Vol. I, 1948.
4. Lighthill, M.J.'On the hodograph transformation for high speed flow. II. A flow with circulation.' Quart. J. Mech. & Appl. Math., Vol. 1,1948.
5. Cherry, T.M.,'Flow of a compressible fluid about a cylinder.' Proc. Roy. Soc.,London, Vol.192, 1947, & Vol. A 196, 1949.
6. Nieuwland, G.Y.,'The computation by Lighthill's method of transonic potential flow around a family of quasi-elliptical aerofoils.' NLR-TR T.83, 1964.
7. Boerstoel, J.W.,'A survey of symmetrical transonic potential flows around quasi-elliptical aerofoil sections.' NLR-TR T.136, 1967.
8. Nieuwland, G.Y.,'Transonic potential flow around a family of quasi-elliptical aerofoil sections' NLR-TR T.172, 1967.
9. Takanashi, S. 'A method of obtaining transonic shock-free flow around lifting aerofoils', Trans. Japan Soc. Aero. Space Sci.,Vol.16, No.34, 1973, and also, 'An exact solution for the transonic potential flow past aerofoil sections', NAL TR. (TO be published; in Japanese).
10. Boerstoel, J.W. and Uijlenhoet, R.,'Lifting aerofoils with supercritical shock-free flow', NLR MP70015U, 1970.
11. Garabedian, P.R. and Korn, D.G.,'Numerical design of transonic airfoils', Numerical solution of partial differential equations. II. Academic Press, New York, 1971.
12. Shigemi, T.,Takeuchi,S.,Takanashi,S.,Suzuki,K., and Nakamura,S.,'Wind-tunnel test of a shock-free lifting aerofoil designed by means of an exact solution of the transonic flow theory', NAL TM (To be published; in Japanese).
13. Ebihara, M., Ishida, Y.,and Okonogi, T.,'A description of the idea underlying a computer program for predicting the aerofoil pressure distribution in sub-critical viscous flow', NAL TR-248, (In Japanese), 1971.
14. Sato, J.,'On peaky aerofoil sections', Jour. Japan Soc. Aero. Space Sci., Vol.18, No.201, (In Japanese), 1970.
15. Kamiya, N.,'On the drag divergence of two-dimentional airfoils at transonic speeds', NAL TR-299, (In Japanese), 1973.

DISCUSSION

D. Brown (National Aeronautical Establishment, Ottawa, Canada): What was the value of the aspect ratio of the model tested in the Ludwieg tube? Was there any removal of the wall boundary layer?

T. Shigemi: The question is in fact related to a certain test result stated in the author's oral presentation and shown in a slide at the 9th ICAS Congress, which is not included in the printed material. For the convenience of readers, the author will reproduce here the point under discussion and the test result in question (see Fig. 5').

The local Mach number distribution on the 7523-10 section at nearly shock-free flow condition is indicated as Fig.5 in this material: that is the test result obtained in NAL 2mx2m Transonic Wind Tunnel. Referring to the Reynolds number ($\approx 5 \times 10^6$, based on the chord length) of this test, the author added that a test result with a little higher Reynolds number (14×10^6) of the same aerofoil section had recently been obtained by K. Takashima using NAL's pilot Ludwieg tube of 12cm x 36cm test section. The corresponding data by this Ludwieg tube were plotted in symbols Δ in Fig. 5' (which was to replace Fig.5), and compared with the former data. From the good agreement of these results at different Reynolds numbers, the author conjectured that, as far as the nearly shock-free condition (which these tests stand for) was concerned, the pressure distribution did not seem to suffer so much from the Reynolds-number effects.

Now, coming back to the point of question, the author supplements his comment saying that the size of the model tested in the Ludwieg tube was 12cm span and 14cm chord; hence the value of the aspect ratio was less than unity. Removal of the side-wall boundary layer was not yet provided, since the two-dimensional test in the Ludwieg tube at NAL was presently at the preliminary stage.

As this model may be considered somewhat over-sized, there might be certain questions in respect of the two-dimensionality of the flow (as the writer suggests) and also of the blockage ratio, in addition to the other well-known difficulties in testing an aerofoil at supercritical state. However, such oversize model would be justifiable sometimes under limited test conditions; shock-free and comparatively low lift conditions, for instance. The author does not think that the agreement of the data was a mere coincidence by chance.

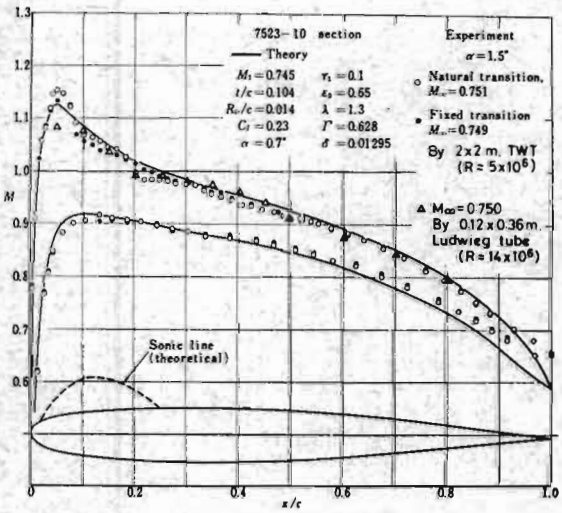

Fig.5'